Supplementary Information

Unveiling Magnetic Transition-Driven Lattice Thermal Conductivity Switching in Monolayer VS_2

Zimmi Singh[1*], Abhishek Kumar[1*], Sankha Mukherjee[1#]
[1]Metallurgical and Materials Engineering Department, Indian Institute of Technology Kharagpur, India
[#]Email: sankha@metal.iitkgp.ac.in
[*]These authors contributed equally

Comparison between the frozen phonon technique and Density functional perturbation theory:

The finite displacement method (frozen phonon approach) [1], [2] and linear response theory using density functional perturbation theory (DFPT) [3], [4] are used to calculate the phonon dispersions relationships.

In this manuscript, the frozen phonon technique was used to calculate the phonon dispersion relationships and other associated properties. These dispersion relationships, shown in Figure S1(b) are compared with those calculated using DFPT methods, as shown in Figure S1(a). From these comparisons, it can be concluded that the dispersion relationships are not dispersed, although a few modes at the K wave vectors are coupled. Additionally, the Raman active and IR active modes at the center of the Brillouin zone match exactly. Furthermore, Raman and IR active modes were compared with the available literature, as shown in Table S1.

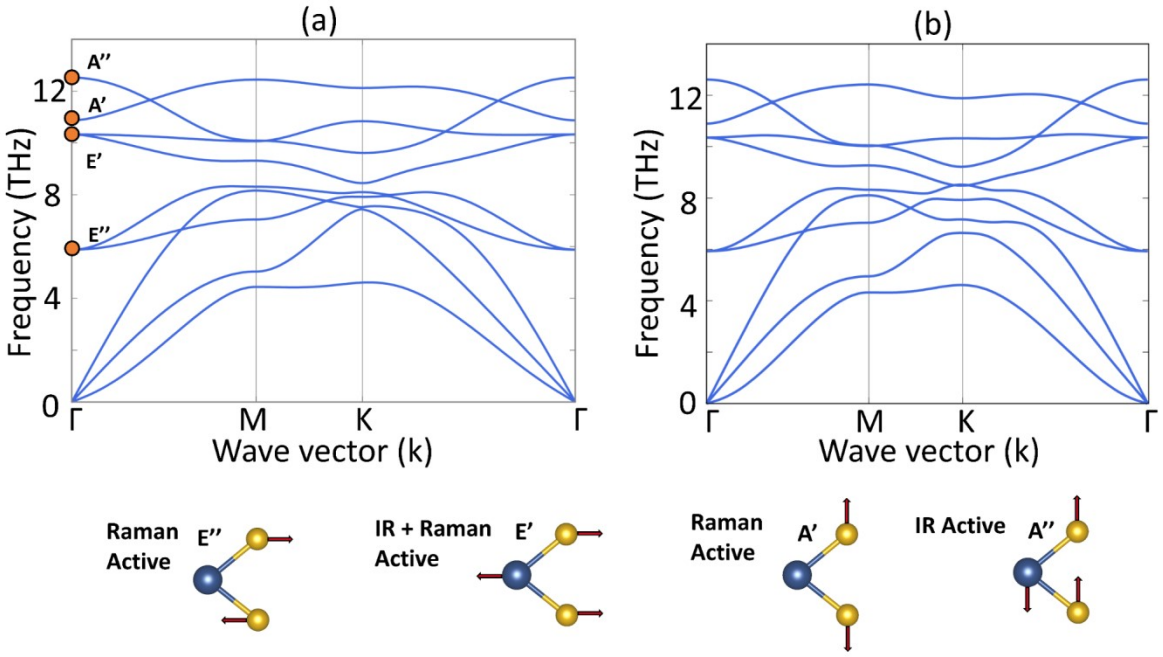

Figure S1: The phonon dispersion is calculated using the linear response technique using density functional perturbation theory (DFPT), shown in Figure (a), and compared with phonon dispersions calculated using the frozen phonon method, shown in Figure (b) for the FM phase of VS_2.

Stress-strain response under uniaxial strain:

In Table S2, we listed the values of elastic constants and Young's modulus at strain steps of 0.3% for ferromagnetic (FM) and paramagnetic (PM) states of VS_2.

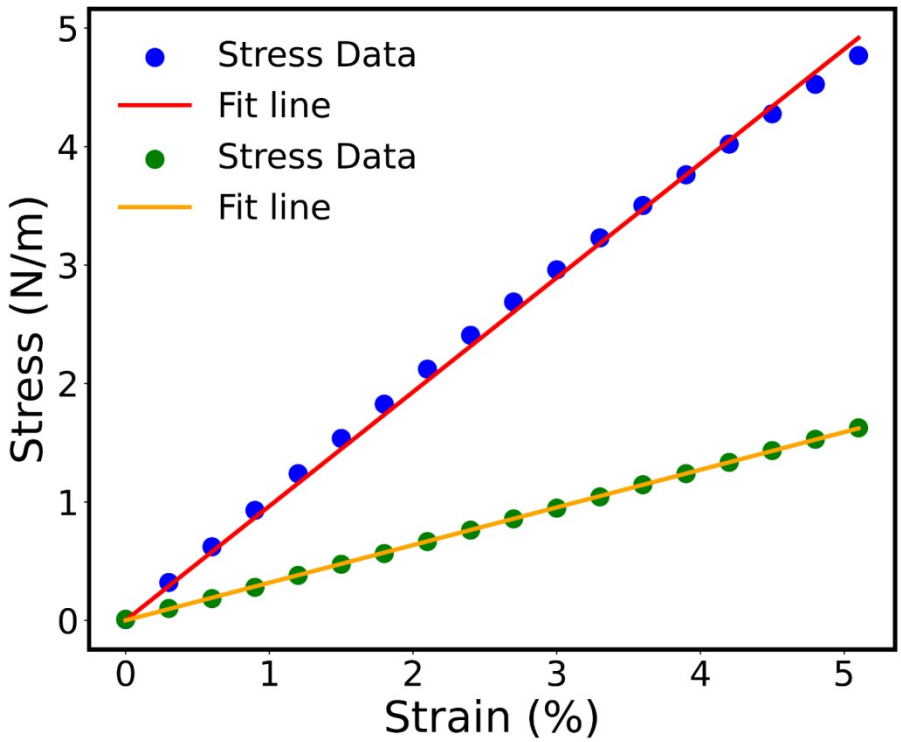

Figure S2: The stress-strain response under uniaxial strain on the FM phase is where straight lines fit stress data points, and the linear elastic constants are calculated from slopes.

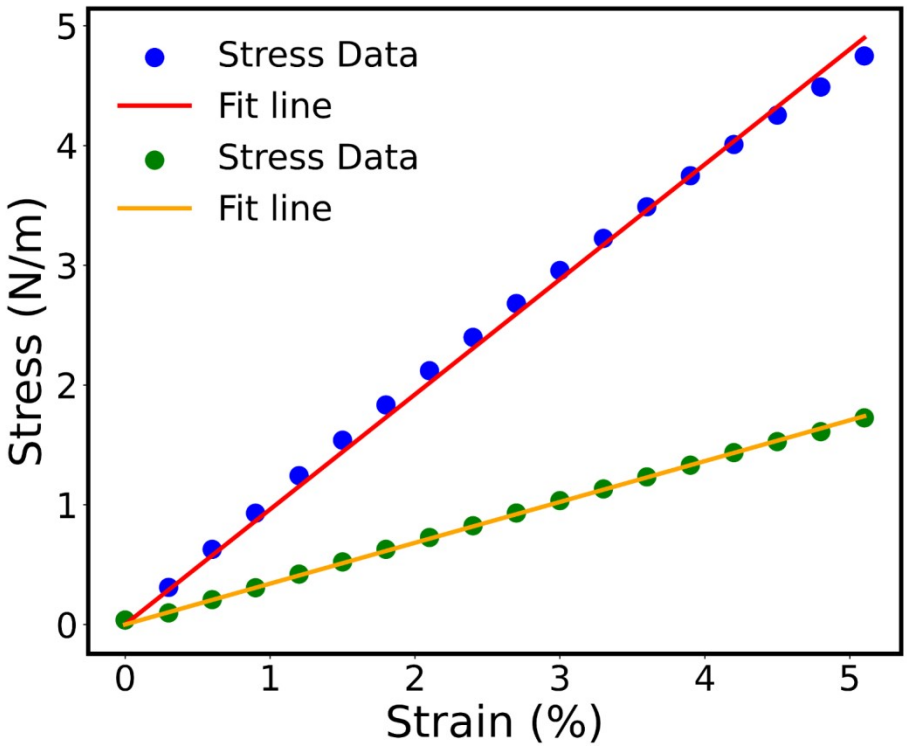

Figure S3: The stress-strain response under uniaxial strain on the PM phase is where straight lines fit stress data points, and the linear elastic constants are calculated from slopes.

κ_{lat} with Isotope scattering:

We performed calculations with and without isotopes and non-analytical term corrections (NAC) on the FM phase. As shown in Figure S4, isotope scattering significantly reduced lattice thermal conductivity (κ_{lat}) across all temperatures, similar to NAC calculations without isotope scattering. However, Born effective charges and dielectric constants had little effect on κ_{lat} with isotope scattering, even when NAC was included in the dynamical matrix. NAC calculations for PM states proved challenging, leading to breakdowns. Therefore, we used isotope scattering without NAC correction for κ_{lat} in this study. As shown in Figure S5, κ_{lat} consistently decreased across all temperatures with isotope scattering in both FM and PM phases.

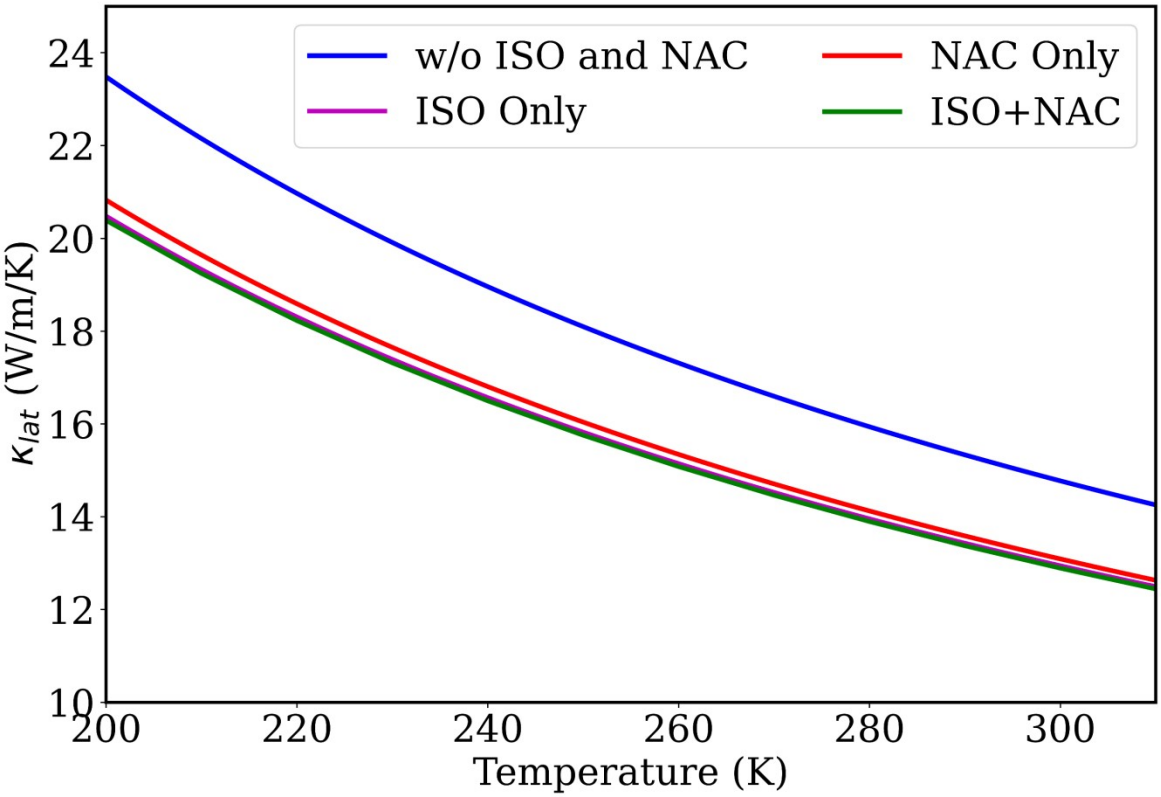

Figure S4: Isotope scattering consistently reduces the κ_{lat} value across the FM phase of VS_2. However, the correction of non-analytical terms (Born effective charges and dielectric constants) associated with isotope scattering has a negligible effect.

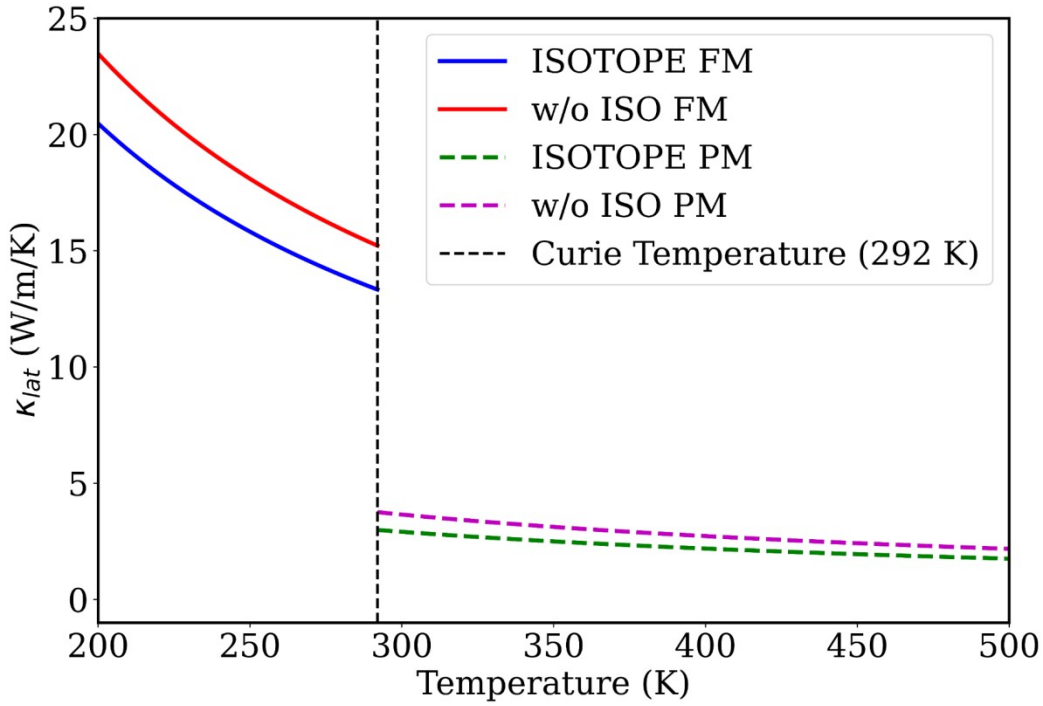

Figure S5: This plot illustrates the κ_{lat} values for both FM and PM phases with and without considering isotope scattering. As evidenced by the data, isotope scattering significantly affects phonon transport, leading to a noticeable reduction in κ_{lat} values.

Stability of structure with AIMD

In the BOMD simulations, the stability of the structure at higher temperatures was assessed. The time history of temperature and total energy showed that both the undeformed and deformed configurations (with 5% strain in the armchair and zigzag directions) of the FM and PM phases remained stable at 292 K and 500 K, respectively, as illustrated in Figure S6-11.

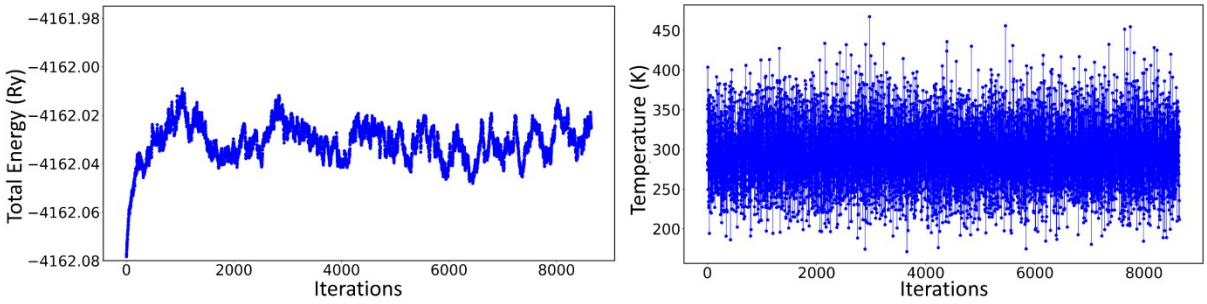

Figure S6: The evolution of total energy (left) and temperature (right) of the FM phase of VS_2.

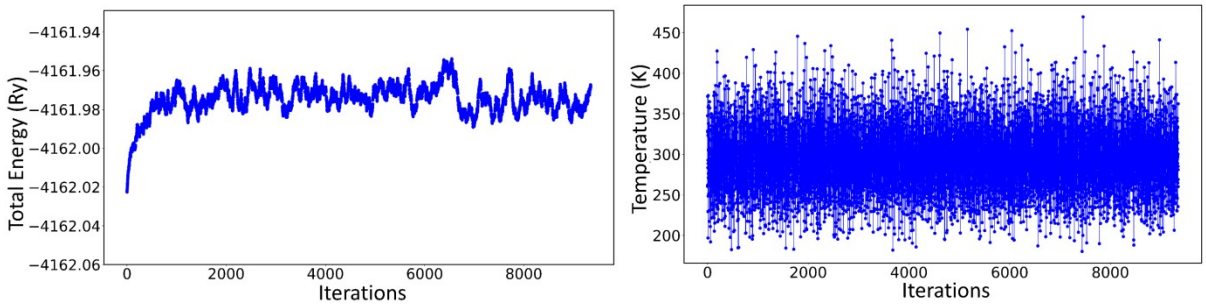

Figure S7: The evolution of total energy (left) and temperature (right) of the FM phase of VS_2 under 5% uniaxial tensile strain in the armchair direction.

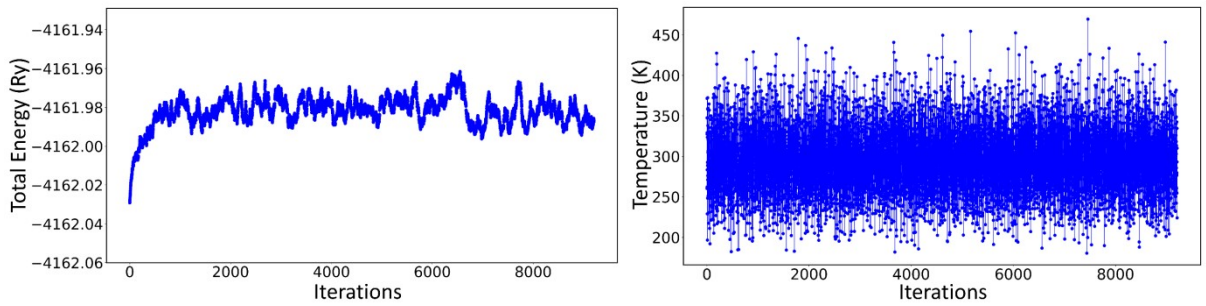

Figure S8: The evolution of total energy (left) and temperature (right) of the FM phase of VS_2 under 5% uniaxial tensile strain in the zigzag direction.

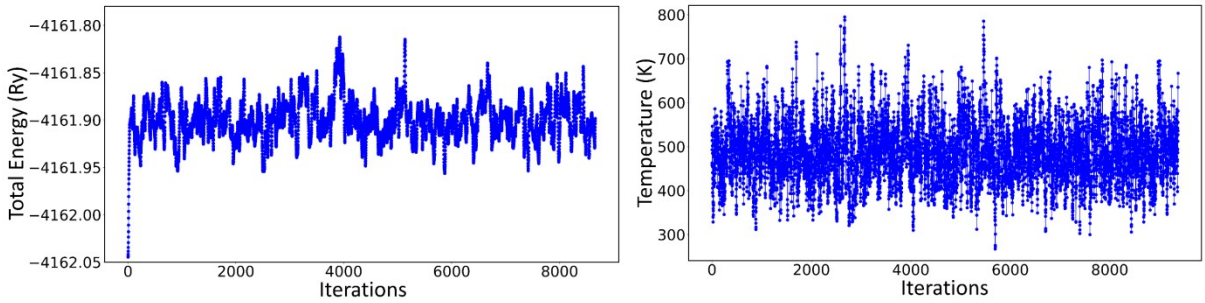

Figure S9: The evolution of total energy (left) and temperature (right) of the PM phase of VS_2.

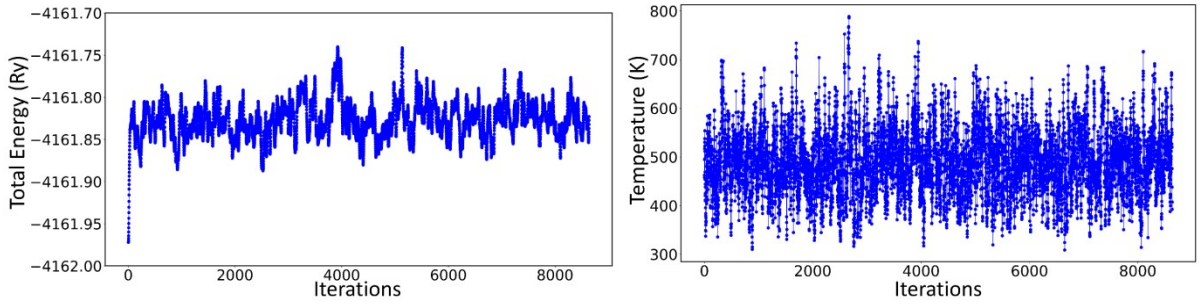

Figure S10: The evolution of total energy (left) and temperature (right) of the PM phase of VS_2 under 5% uniaxial tensile strain in the armchair direction.

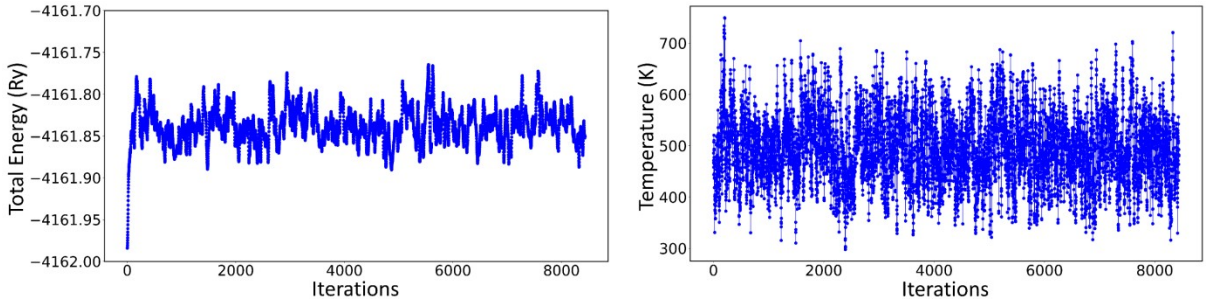

Figure S11: The evolution of total energy (left) and temperature (right) of the PM phase of VS_2 under 5% uniaxial tensile strain in the zigzag direction.

Convergence Tests

The cumulative κ_{lat} value converges at the mean free path at 101×101×1 grid point, though our reported calculations were performed with 151×151×1 grid point. Figure S12 shows that the κ_{lat} value converges with the mean free path.

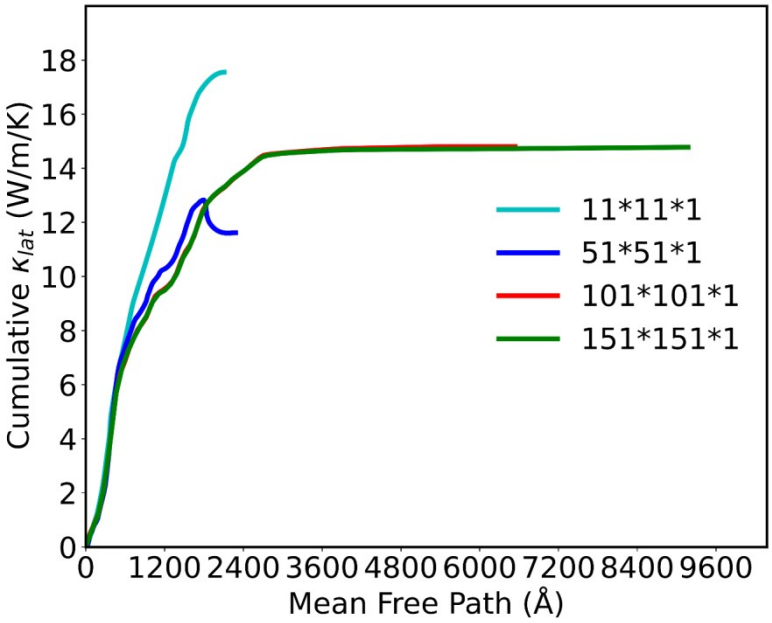

Figure S12: The cumulative κ_{lat} convergence was shown with the mean free path.

Ensuring the convergence of the lattice thermal conductivity (κ_{lat}) value with the Q-grid is essential. Convergence of κ_{lat} for Q-grids in the range between 11×11×1 to 251×251×1 was calculated at a temperature of 292 K for FM and 300 for PM states, as shown in Figure S13. The κ_{lat} value was found to converge for Q-grids consisting of 151×151×1 point, indicating the suitability of the chosen Q-grid. Additionally, as shown in Figure S14, we tested κ_{lat} convergence across a host of temperatures in the range of 200 K- 500 K using Q-grids from 11×11×1 to 251×251×1.

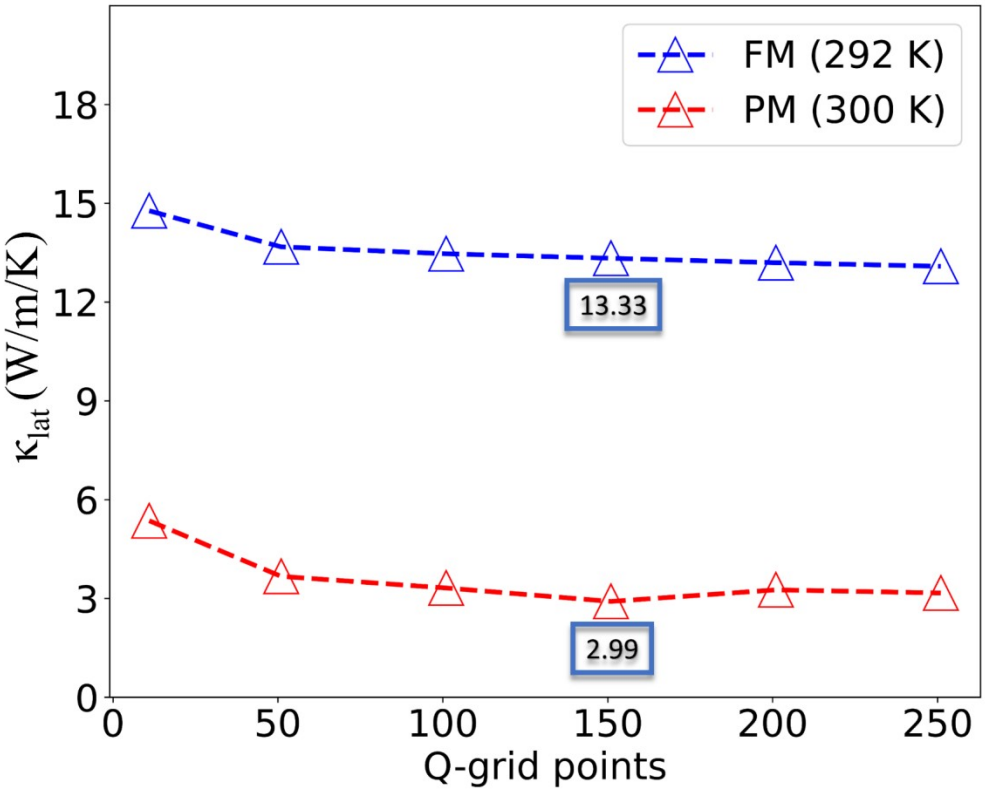

Figure S13: Illustrates the convergence of κ_{lat} value with different Q-grids for both FM and PM phases of VS_2.

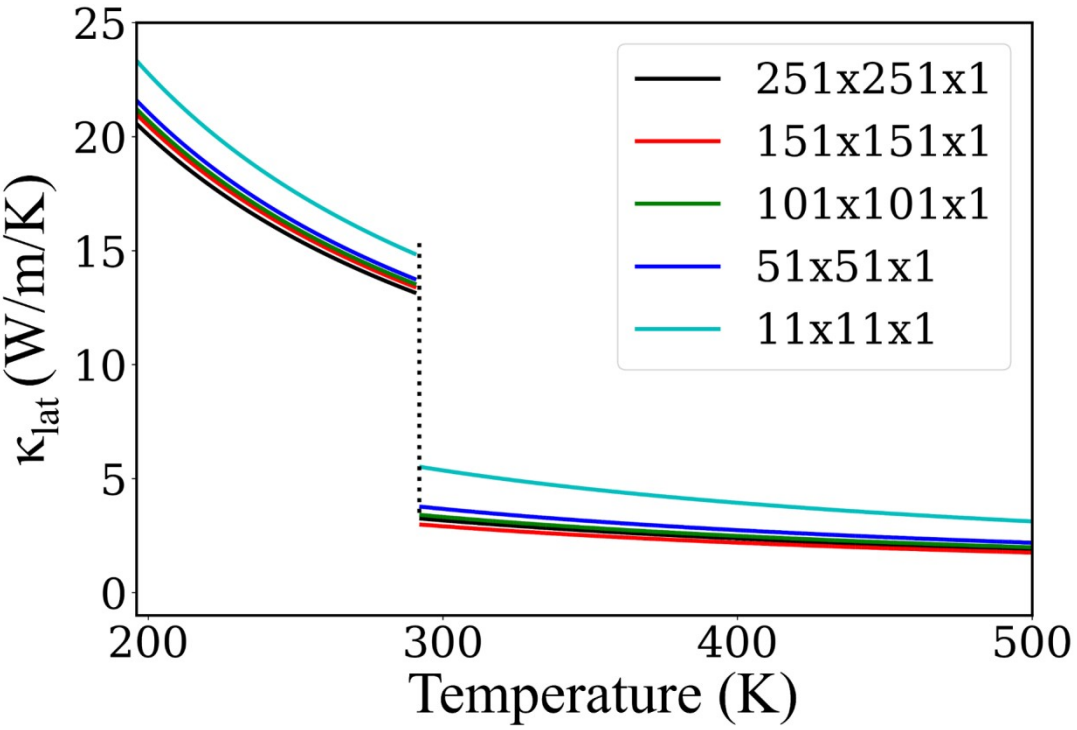

Figure S14: The κ_{lat} was optimized using various q-point meshes across a temperature range of 200 K to 500 K. This optimization was performed for both the FM phase (up to the Curie temperature of 293 K) and the PM phase (above the Curie temperature).

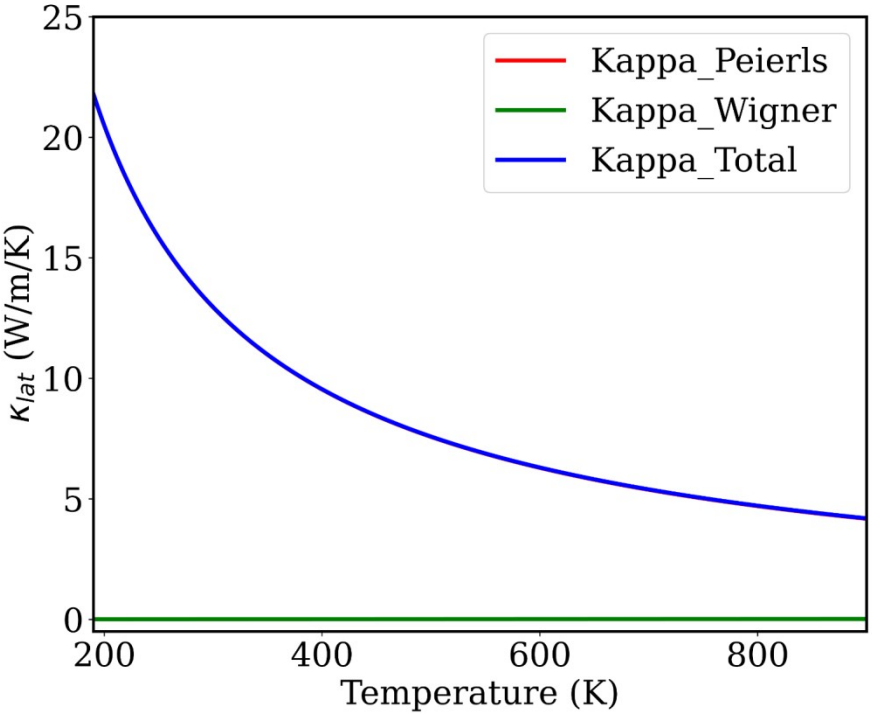

Figure S15: The total κ_{lat} of FM phase variation with temperature is shown where transportation of phonons is treated as particle-like (kappa_Peierls) and wave-like (Kappa_Wigner).

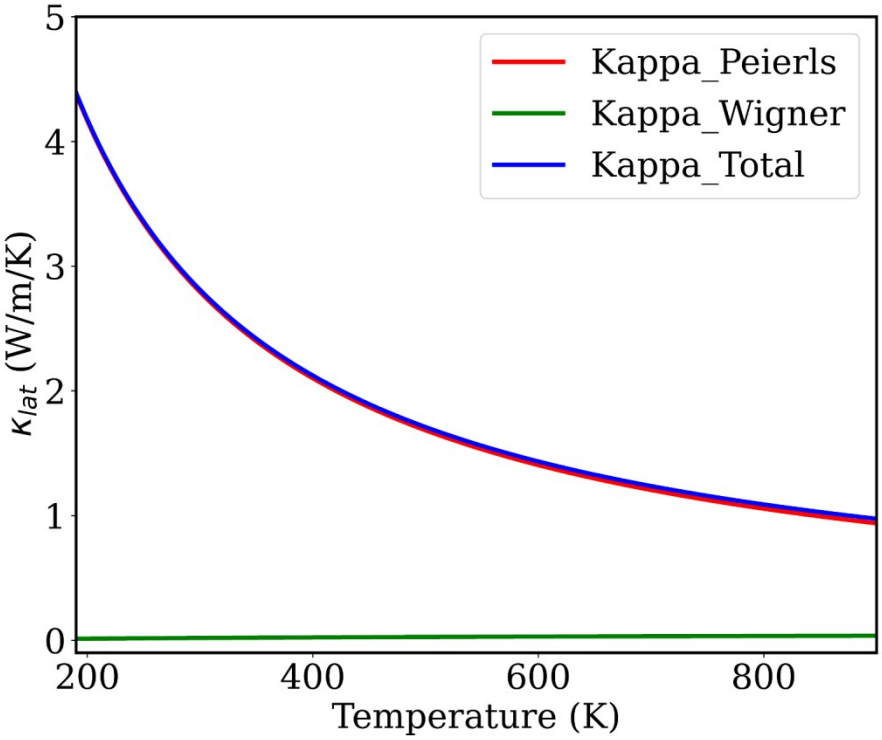

Figure S16: The total κ_{lat} of PM phase variation with temperature is shown where transportation of phonons is treated as particle-like (kappa_Peierls) and wave-like (Kappa_Wigner).

Table S1: Raman and IR active modes of FM VS_2 in the THz unit are shown in the above table (calculated from DFPT). Herin, we have compared its values with those of the available theoretical and experimental literature.

FM_VS_2	**A''**	**A'**	**E'**	**E''**
Ref. [5]	12.88	11.37	7.42	5.98
Ref. [6]	13.56	11.50	7.70	6.47
Ref. [7]	12.15	10.54	9.82	5.81
Exp. Ref. [8]		12.12	11.52	
Exp. Ref. [9]		12.18	11.67	
Our Work (DFPT)	12.51	10.87	10.32	5.88

Table S2: The values of elastic constants and Young's modulus at strain steps of 1% and 0.3%.

VS_2	C_{11} (N/m)	C_{12} (N/m)	E (N/m)
FM	96.4089	31.8	85.9
PM	96.0261	34.1	83.9

References

[1] G. Kresse, J. Furthmuller, and J. " Er, "Ab initio Force Constant Approach to Phonon Dispersion Relations of Diamond and Graphite," 1995.

[2] K. Parlinski, Z. Q. Li, and Y. Kawazoe, "First-Principles Determination of the Soft Mode in Cubic ZrO 2," 1997.

[3] P. Giannozzi, S. De Gironcoli, P. Pavone, and S. Baroni, "Ab initio calculation of phonon dispersions in semiconductors," 1991.

[4] X. Gonze and C. Lee, "Dynamical matrices, Born effective charges, dielectric permittivity tensors, and interatomic force constants from density-functional perturbation theory," 1997.

[5] E. B. Isaacs and C. A. Marianetti, "Electronic correlations in monolayer VS_2," Feb. 2016, doi: 10.1103/PhysRevB.94.035120.

[6] H. L. Zhuang and R. G. Hennig, "Stability and magnetism of strongly correlated single-layer VS2," *Phys Rev B*, vol. 93, no. 5, Feb. 2016, doi: 10.1103/PhysRevB.93.054429.

[7] H. J. Wu, Y. L. Wan, Z. Y. Zeng, C. E. Hu, X. R. Chen, and H. Y. Geng, "Ferromagnetic vanadium disulfide VS_2 monolayers with high Curie temperature and high spin polarization," *Physical Chemistry Chemical Physics*, vol. 25, no. 14, pp. 10143–10154, 2023, doi: 10.1039/d3cp00377a.

[8] J. Su *et al.*, "Sub-Millimeter-Scale Monolayer p-Type H-Phase VS2," *Adv Funct Mater*, vol. 30, no. 17, pp. 1–9, 2020, doi: 10.1002/adfm.202000240.

[9] W. Fang, H. Zhao, Y. Xie, J. Fang, J. Xu, and Z. Chen, "Facile Hydrothermal Synthesis of VS2/Graphene Nanocomposites with Superior High-Rate Capability as Lithium-Ion Battery Cathodes," *ACS Appl Mater Interfaces*, vol. 7, no. 23, pp. 13044–13052, 2015, doi: 10.1021/acsami.5b03124.

[10] P. Giannozzi *et al.*, "QUANTUM ESPRESSO: A modular and open-source software project for quantum simulations of materials," *Journal of Physics Condensed Matter*, vol. 21, no. 39, 2009, doi: 10.1088/0953-8984/21/39/395502.

[11] J. P. Perdew, K. Burke, and M. Ernzerhof, "Generalized gradient approximation made simple," *Phys Rev Lett*, vol. 77, no. 18, pp. 3865–3868, 1996, doi: 10.1103/PhysRevLett.77.3865.

[12] J. P. Perdew and Y. Wang, "Erratum: Accurate and simple analytic representation of the electron-gas correlation energy (Physical Review B (1992) 45 (13244) DOI:

10.1103/PhysRevB.45.13244)," *Phys Rev B*, vol. 98, no. 7, pp. 244–249, 2018, doi: 10.1103/PhysRevB.98.079904.

[13] K. F. Garrity, J. W. Bennett, K. M. Rabe, and D. Vanderbilt, "Pseudopotentials for high-throughput DFT calculations," May 2013, doi: 10.1016/j.commatsci.2013.08.053.

[14] B. X. Shi, R. J. Nicholls, and J. R. Yates, "Accurate and efficient structure factors in ultrasoft pseudopotential and projector augmented wave DFT," Sep. 2022, [Online]. Available: http://arxiv.org/abs/2209.12227

[15] H. R. Fuh, C. R. Chang, Y. K. Wang, R. F. L. Evans, R. W. Chantrell, and H. T. Jeng, "Newtype single-layer magnetic semiconductor in transition-metal dichalcogenides VX 2 (X = S, Se and Te)," *Sci Rep*, vol. 6, Sep. 2016, doi: 10.1038/srep32625.

[16] G. K. H. Madsen and D. J. Singh, "BoltzTraP. A code for calculating band-structure dependent quantities," *Comput Phys Commun*, vol. 175, no. 1, pp. 67–71, 2006, doi: 10.1016/j.cpc.2006.03.007.

[17] S. Chaudhuri, A. Bhattacharya, A. K. Das, G. P. Das, and B. N. Dev, "Strain Driven Anomalous Anisotropic Enhancement in the Thermoelectric Performance of monolayer MoS 2."